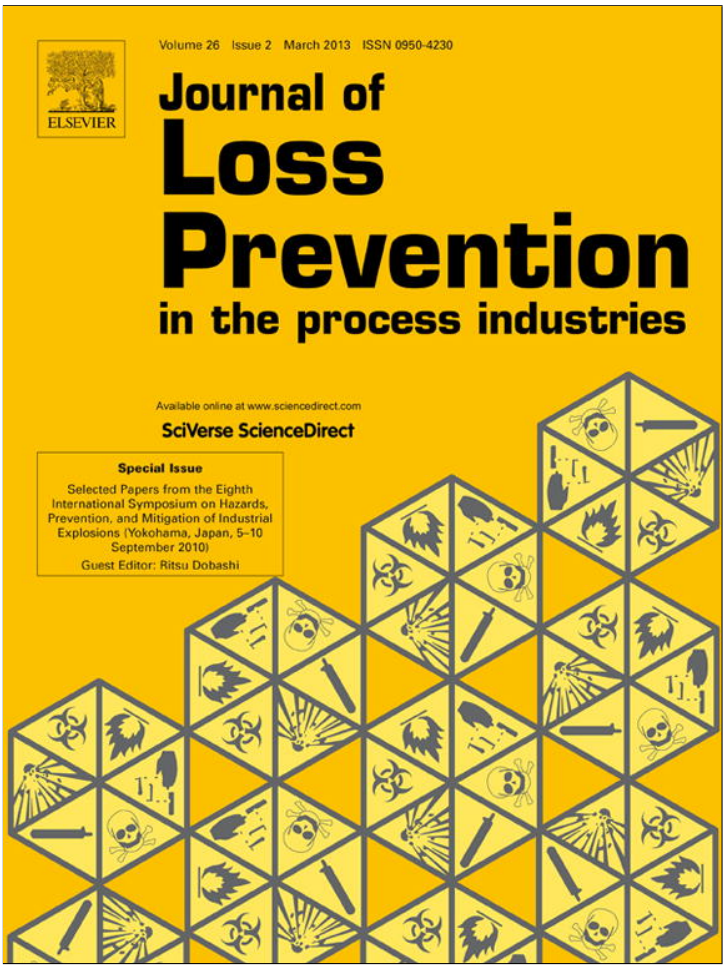

Journal of Loss Prevention in the Process Industries 26 (2013) 302–309

Contents lists available at SciVerse ScienceDirect

Journal of Loss Prevention in the Process Industries

journal homepage: www.elsevier.com/locate/jlp

Numerical simulation of flame propagation and localized preflame autoignition in enclosures

S.M. Frolov [a,*], V.S. Ivanov [a], B. Basara [b], M. Suffa [b]

[a] Department of Combustion and Explosion, N. Semenov Institute of Chemical Physics, 4, Kosigin Street, 119991 Moscow, Russian Federation
[b] Advanced Simulation Technologies, AVL LIST GmbH, Austria

ARTICLE INFO

Article history:
Received 21 November 2010
Received in revised form
17 September 2011
Accepted 26 September 2011

Keywords:
Frontal and volumetric combustion
Enclosure
Numerical simulation

ABSTRACT

A novel computational approach based on the coupled 3D Flame-Tracking–Particle (FTP) method is used for numerical simulation of confined explosions caused by preflame autoignition. The Flame-Tracking (FT) technique implies continuous tracing of the mean flame surface and application of the laminar/turbulent flame velocity concepts. The Particle method is based on the joint velocity–scalar probability density function approach for simulating reactive mixture autoignition in the preflame zone. The coupled algorithm is supplemented with the database of tabulated laminar flame velocities as well as with reaction rates of hydrocarbon fuel oxidation in wide ranges of initial temperature, pressure, and equivalence ratio. The main advantage of the FTP method is that it covers both possible modes of premixed combustion, namely, frontal and volumetric. As examples, combustion of premixed hydrogen–air, propane–air, and *n*-heptane–air mixtures in enclosures of different geometry is considered. At certain conditions, volumetric hot spots ahead of the propagating flame are identified. These hot spots transform to localized exothermic centers giving birth to spontaneous ignition waves traversing the preflame zone at very high apparent velocities, i.e., nearly homogeneous preflame explosion occurs. The abrupt pressure rise results in the formation of shock waves producing high overpressure peaks after reflections from enclosure walls.

1. Introduction

Numerical simulation of flame propagation with preflame autoignition in enclosures is a complex problem. The phenomenology of the process includes flame ignition and propagation, unburned mixture compression and heating, as well as formation of hot spots and fast-spreading localized explosions in the preflame region. The localized explosions evolve from the sites with the minimum induction time and traverse the preflame zone as spontaneous ignition waves with the propagation velocity depending on the local instantaneous distributions of temperature and mixture composition. Better understanding of these phenomena is important for the improvement of existing measures aimed at preventing violent accidental explosions in process plants.

The objective of any combustion model in a CFD code is to provide correct values of mean reaction rates in each computational cell regardless the combustion mode (premixed, nonpremixed, partially premixed, homogeneous, inhomogeneous, spontaneous, frontal, etc.). The correct value of the mean reaction rate in the computational cell can be obtained only if one knows the reaction kinetics and instantaneous fields of temperature and species concentrations inside the cell. The development of reaction kinetics is the separate task which is independent of the CFD combustion modeling. The only relevant issue is the CPU time required for calculating instantaneous reaction rates. This issue can be overcome by applying properly validated short overall reaction mechanisms or look-up tables.

The instantaneous fields of temperature and species concentrations inside the cell are usually not known. Therefore, one has to replace this lacking information by combustion models. There exist many combustion models both for laminar and turbulent flows. If combustion chemistry is fast as compared to mixing, the Spalding (1976) Eddy-Break-Up model can be used. It is simple but has a limited range of validity. There is a whole class of statistical combustion models (based on the formalism of probability density functions (PDF)) with probabilistic representation of turbulence and its interaction with chemistry, Pope (1990). This approach is very attractive for treating both flame propagation and autoignition problems, however requires large CPU resources. The other class of models deals with a flamelet approach, Peters (1986). In this

* Corresponding author. Tel.: +7 495 9397228; fax: +7 495 6512191.
E-mail addresses: smfrol@chph.ras.ru, sergei@frolovs.ru (S.M. Frolov).

0950-4230/$ – see front matter © 2011 Elsevier Ltd. All rights reserved.
doi:10.1016/j.jlp.2011.09.007

Table 1
Some correlations for function F in the relationship for turbulent flame velocity u_t.

No.	Correlation	Reference
1	$F = 1 + \frac{u'}{u_n}$	Damkoehler (1940)
2	$F = \left(1 + \frac{u'^2}{u_n^2}\right)^{1/2}$	Shchelkin (1949)
3	$F = 1 + 0.52\left(\frac{u'}{u_n}\right)^{1/2}\left(\frac{u'l}{\nu}\right)^{1/4}$	Zimont (1979)
4	$F = 1 + 0.62\left(\frac{u'}{u_n}\right)^{1/2}\left(\frac{u_n l}{\nu}\right)^{1/4}$	Gülder (1990)
5	$F = 1 + 0.95\mathrm{Le}^{-1}\left(\frac{u'}{u_n}\right)^{0.5}\left(\frac{l}{\delta}\right)^{0.5}$	Bradley (1992)
6	$F = 1 + 0.435\left(\frac{u'}{u_n}\right)^{0.4}\left(\frac{u_n l}{\nu}\right)^{0.44}$	Liu, Ziegler, and Lenze (1993)
7	$F = -0.274\left(1 + \frac{u_n l}{\nu}\right) + \left(0.076\left(1 + \frac{u_n l}{\nu}\right)^2 + 0.547\left(1 + \frac{u_n l}{\nu}\right)\frac{u'}{u_n} + 1.547\right)^{0.5}$	Peters (1999)

Notations: ν is molecular kinematic viscosity, Le is the Lewis number.

approach, the instantaneous flame is assumed to consist of localized reactive sheets, which are transported by the flow and wrinkled by turbulent eddies. The flamelet approach is applicable when the characteristic turbulent scales are larger than a typical flame thickness. This condition is satisfied in many practical situations.

The approach supposed below is a sort of combination of flamelet and statistical combustion models to allow for simultaneous treatment of frontal combustion by explicit tracing of mean reactive surfaces and volumetric combustion by the transported PDF approach. The availability of such an approach makes it possible to attack the problem of flame propagation with preflame autoignition in enclosures.

2. Flame-tracking method

The FT method deals with the subgrid model of laminar/turbulent combustion. The essence of the model can be readily explained on the example of laminar flame propagation. In the FT method, the flame-surface shape and area are found based on the Huygens principle: Each elementary portion of the flame surface displaces in time due to burning of the fresh mixture at local velocity u_n (normal to the flame surface) and due to convective motion of the mixture at local velocity V. The local instantaneous flame velocity u_n is taken from look-up tables including in general the effects of mixture dilution with combustion products, flame stretching, and flammability limits. The local instantaneous velocity V is calculated using a high-order interpolation technique. In 2D flow approximation, the flame surface is represented by straight line segments, whereas in 3D calculations, the flame surface is represented by connected triangles.

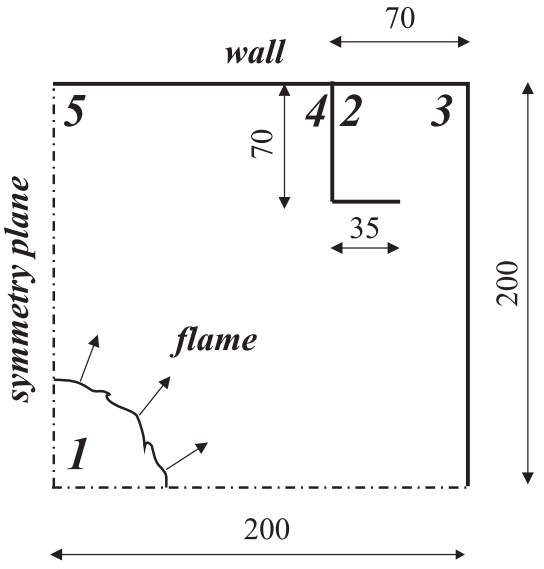

Fig. 1. Computational domain for square enclosure with "room." Points #1 to #5 denote the monitoring locations for flow parameters. Dimensions are in millimeters.

The energy release rate in the computational cell, $\dot{Q}$, is composed of two terms: energy release due to frontal combustion, $\dot{Q}_f$, and energy release due to volumetric reactions, $\dot{Q}_v$. The first term $\dot{Q}_f$ is calculated based on the estimated instantaneous flame-surface area S_n, fresh mixture density ρ, and laminar flame propagation velocity u_n:

$$\dot{Q}_f = \rho Q \sum S_{ni} u_{ni} \tag{1}$$

where Q is the combustion heat and summation is made over all flame segments in the cell. The second term $\dot{Q}_v$ is calculated using a Particle method (see below).

In the turbulent flow field, a pulsating velocity vector distorts the "mean" reactive (flame) surface by wrinkling it. The local instantaneous flame wrinkling can be taken into account by proper increasing the normal flame velocity, or in other words, by introducing a concept of local turbulent flame velocity u_t. The local turbulent flame velocity is defined as

$$u_t = u_n S / S_n$$

where S is the surface area of the wrinkled flame at a given segment, and S_n is the surface area of the equivalent "planar" flame segment.

The problem now is to find the way of calculating u_t. In the theory of turbulent combustion, there are many correlations between u_t and u_n. A typical correlation yields u_t as a function of u_n and laminar flame thickness $\delta = a/u_n$ (a is the thermal diffusivity), turbulence intensity u' and length scale l, etc.:

$$\frac{u_t}{u_n} = F\left(\frac{u'}{u_n}, \frac{l}{\delta}, \ldots\right) \tag{2}$$

Table 2
Predicted (unstretched) laminar burning velocities (in cm/s) for stoichiometric hydrogen–air mixture at different initial pressures and temperatures.

T_0, K	p, atm					
	1	3	6	10	40	100
293	222	221	215	177	88	36
450	454	477	489	417	235	103
600	783	860	922	807	536	239
800	1445	1666	1875	1679	1293	722

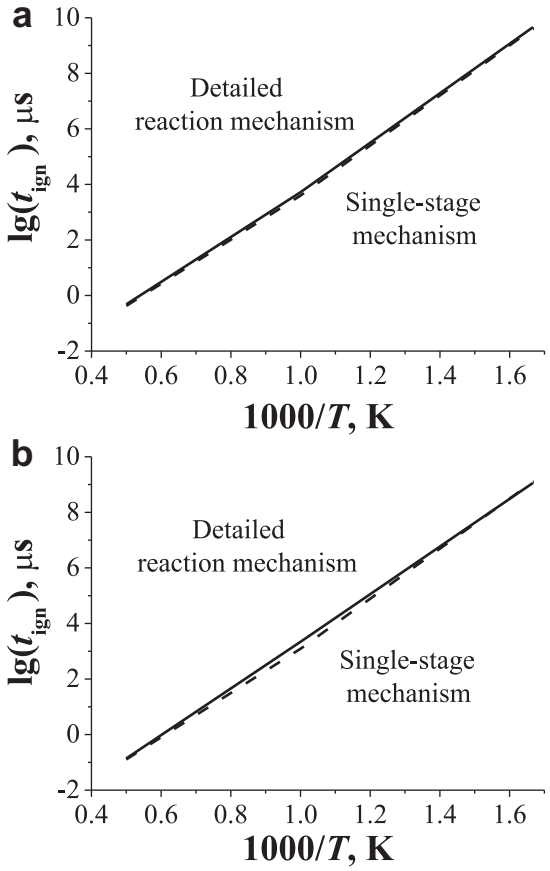

Fig. 2. Ignition delay of stoichiometric hydrogen–air mixture as a function of temperature predicted by detailed reaction mechanism (solid curve) and single-stage mechanism of Eq. (8) (dashed curve): (a) $p = 1$ MPa, (b) $p = 4$ MPa.

where function F is different for different models. Some examples are presented in Table 1. All formulas for u_t in Table 1 are asymptotically valid for laminar combustion (when $u' \to 0$, $u_t \to u_n$). Note that the correlations of Table 1 have been obtained based on the unstretched laminar flame velocity u_n. As a matter of fact, u_n can be affected by stretching and quenching in the turbulent flow field (Driscoll, 2008). Unfortunately, available models of these effects are mainly phenomenological, include a number of uncertain input parameters, and have not been reliably validated.

Thus, Huygens principle can be applied to model the "mean" shape of the turbulent flame: each elementary portion of flame surface displaces in time due to burning of the fresh mixture at local velocity u_t (normal to the flame surface) and due to convective motion of the mixture at local velocity V. The subgrid model of turbulent premixed combustion does not differ much from that of the laminar premixed combustion, except for using u_t instead of u_n in Eq. (1).

The main problem in implementing such a combustion model into a CFD code is the development of an efficient algorithm for explicit "mean" flame-surface tracing inside computational cells. This algorithm should meet the constraints on the flame-front continuity, connectivity, etc., as well as the constraints on the CPU time.

The detailed description of the FT method can be found elsewhere (Frolov & Ivanov, 2010; Ivanov & Frolov, 2010).

3. Particle method

The preflame zone exhibits volumetric reactions of fuel oxidation, formation of intermediate products like alcohols, aldehydes, peroxides, etc. In general, preflame reactions are inhomogeneous due to inhomogeneous distributions of temperature and main species concentrations and due to high sensitivity of reaction rates to these parameters. Therefore preflame reactions can result in localized energy release.

Direct (and CPU time consuming) way to calculate volumetric reaction rates is to solve the equations of chemical kinetics in the preflame zone in each computational cell. To shorten the CPU time, we introduce a certain number of notional Lagrangian particles which move in the preflame zone according to the local instantaneous velocity vector. In each particle, preflame reactions proceed at the rates determined by its instantaneous temperature and species concentrations. For determining the time and location of preflame autoignition, a certain autoignition criterion is adopted. The criterion is based on the fixed rate of temperature rise in the particle, e.g., 10^6 K/s.

The mean energy release rate $\dot{Q}_v$ (averaged over all particles in cell) directly affects the mean flow pattern. When the autoignition criterion is met in one or several particles, a new (forced) ignition site in the preflame zone is automatically introduced. In general, these ignition sites give birth to new laminar/turbulent flame kernels or, if the preflame reactions are fast, they result in the induction (spontaneous, Zel'dovich, 1980) flames and volumetric combustion. For keeping the number of particles at a reasonable level, the consistent procedures of particle cloning and clustering are developed. The preflame particles are traced until the entire geometry is traversed by the frontal or volumetric combustion.

In each ith Lagrangian particle, the following set of equations is solved (Frolov & Ivanov, 2010):

$$\frac{dx_k^i}{dt} = u_k^i \tag{3}$$

$$\frac{d\left(\rho_l^i V^i\right)}{dt} = \nabla \vec{J}_l^i + J_{l,\mathrm{hom}}^i \tag{4}$$

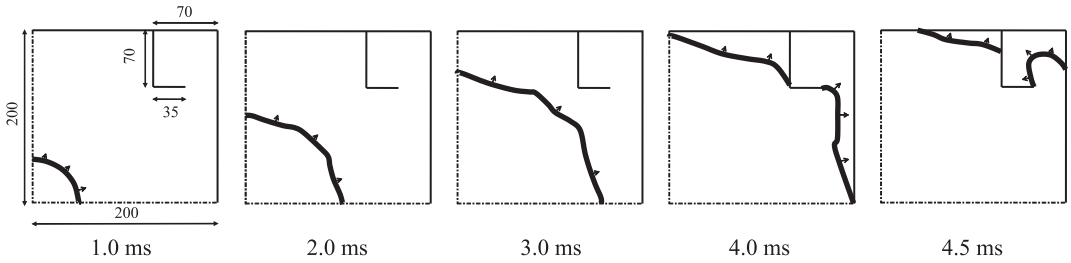

Fig. 3. Snapshots of hydrogen–air flame propagation in the enclosure.

$$\rho^i \frac{\mathrm{d}\vec{u}_k^i}{\mathrm{d}t} = \frac{\partial P^i}{\partial x_k} - \nabla\left(Ep^i + \tau^i\right) \quad (5)$$

$$\rho^i \frac{\mathrm{d}h^i}{\mathrm{d}t} = -\nabla\vec{q}^i + h^i_{\mathrm{hom}} + \frac{\partial P^i}{\partial t} - P\frac{\partial u_k^i}{\partial x_k} \quad (6)$$

where x_k^i is the coordinate ($k = 1$, 2, and 3) and u_k^i is the velocity component, ρ_l^i is the partial density of the lth species, ρ^i is the mean particle density, V^i is the particle volume, $\nabla\vec{J}_l^i$ is the diffusion flux of the lth species to/from the particle, and $J^i_{l,\mathrm{hom}}$ is the flux of the lth species due to chemical reaction, P^i is the mean pressure, p^i is the pulsating pressure, E is the unit tensor, and τ^i is the molecular viscous stress, h^i is the particle enthalpy, $\vec{q}^i$ is the heat flux to/from the particle, h^i_{hom} is the rate of heat deposition due to chemical reactions, $\partial P^i/\partial t$ is particle heating due to adiabatic compression, and $P\partial u_k^i/\partial x_k$ is particle heating due to shock compression.

Molecular diffusion term $\nabla\vec{J}^i$ in Eq. (4), molecular heat transfer term $\nabla\vec{q}^i$ in Eq. (6) and term $\partial p^i/\partial' x_k + \nabla\tau$ in Eq. (5) are modeled using classical models of Interaction by Exchange with the Mean (Pope, 1985):

$$\nabla J_l^i = -0.5C_1\left(Y_l^i - \overline{Y}_l^i\right)\rho^i V^i \omega$$

$$\nabla q^i = -0.5C_2\left(h^i - \overline{h}^i\right)\rho^i\omega$$

$$\left(\rho^i\right)^{-1}\nabla\left(p^i E + \tau^i\right) = -\zeta\left(u_k^i - \overline{u}_k^i\right) + A(t)$$

where C_1 and C_2 are the coefficients ($C_1 \approx C_2 \approx 2{,}0$), Y_l^i is the concentration of the lth species, $\overline{Y}_l^i$ is the mean concentration of the lth species at the location of the ith particle, ω is the turbulent frequency, h^i is the enthalpy, $\overline{h}^i$ is the mean enthalpy at the location of the ith particle, $\overline{u}_k^i$ is the mean kth velocity component at the location of the ith particle, ζ is the coefficient ($\zeta \approx 2075\omega$), and $A(t)$ is the stochastic function in the Langevin equation.

The main advantage of the Particle method is that chemical terms $J^i_{l,\mathrm{hom}}$ and h^i_{hom} in Eqs. (4) and (6) do not require modeling, i.e. there is no need to introduce a particular model for turbulence–chemistry interaction. The Particle method is implemented in the CFD code by splitting physical and chemical processes and solving Eqs. (3)–(6) explicitly. Chemical processes are solved implicitly using the internal time step.

4. Results and discussion

Described below are the results of application of the FTP method to several test cases illustrating method capabilities.

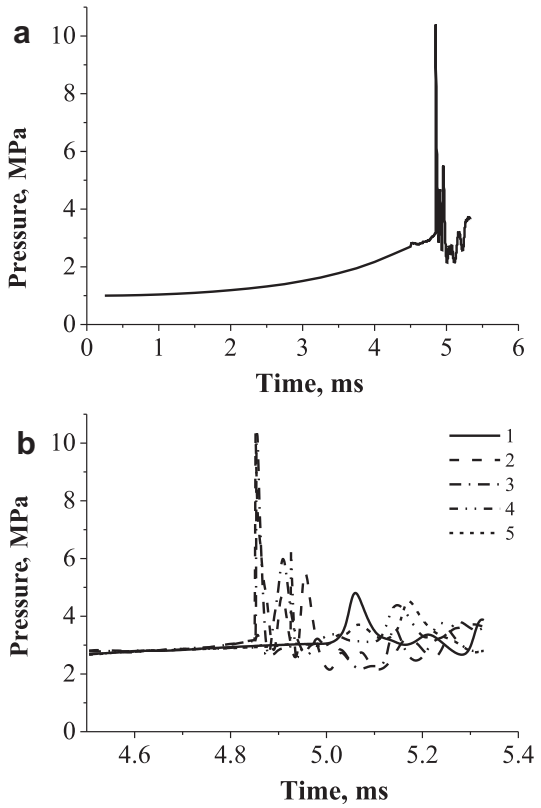

Fig. 5. Predicted pressure histories in monitoring locations #2 (a) and #1 to #5 (b).

4.1. Hydrogen combustion in enclosure of complex shape

Fig. 1 shows a quarter of a square enclosure with the side wall 0.4 m long initially filled with the stoichiometric hydrogen–air mixture at elevated pressure ($p_0 = 1$ MPa) and temperature ($T_0 = 850$ K). The square enclosure contains a square internal "room" 70 × 70 mm with a "door" 35 mm wide. The wall temperature is kept constant and equal to 293 K.

In the course of 2D calculations, the number of flame elements per computational cell is controlled to be 10 ± 2. The mean number of notional particles per cell is kept equal to 10 with the minimum and maximum allowable numbers of particles equal to 6 and 15, respectively. The initial flame kernel is assumed to be a circle 1 mm in radius with the center located in the symmetry center of the enclosure. Initially, the ignition kernel is assumed to be filled with combustion products at thermodynamic combustion temperature and $p = p_0$.

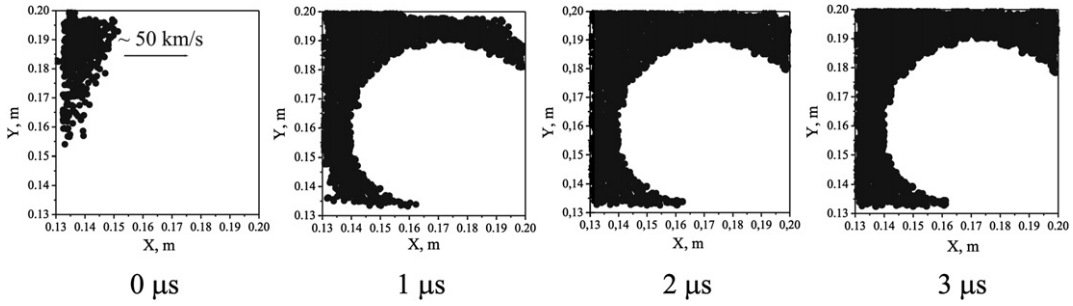

Fig. 4. Snapshots of preflame autoignition in the internal "room" of the enclosure. Time intervals are counted from first autoignition events at ~4.85 ms.

Table 3
Predicted (unstretched) laminar burning velocities (in cm/s) for stoichiometric propane–air mixture at different initial pressures and temperatures.

T_0, K	p, atm				
	1	3	10	40	100
293	39	28	19	8.9	6
450	78	55	35	19	13
600	143	102	64	36	24
750	247	178	112	62	41
900	451	306	191	105	69

For calculating u_t according to Eq. (2), a simple classical correlation of Shchelkin (1949) from Table 1 is used:

$$u_t \approx u_n \sqrt{1 + u'^2/u_n^2} \tag{7}$$

The local turbulence intensity u' is assumed to be related to the turbulent kinetic energy k as $u' = (2k/3)^{1/2}$. Instead of Eq. (7) one can use other available correlations for the turbulent flame velocity which include a local turbulence length scale and laminar flame thickness.

The laminar flame velocity entering Eq. (7) is linearly interpolated using the data of look-up tables for hydrogen (Belyaev et al., 2010). Table 2 shows a small fragment of such a look-up table for the stoichiometric hydrogen–air mixture at different initial pressures and temperatures (shown in the table are only some selected values of p, T_0 and u_n). The table has been constructed based on the numerical solution of the problem of one-dimensional planar (unstretched) laminar flame structure with the detailed chemistry of hydrogen oxidation. The effect of flame stretch on u_n is not included in this particular case. Contrary to this database, the database of stretched laminar flames is based on the numerical solution of the problem of quasi-one-dimensional structure of a counter-flow premixed laminar flame.

Turbulence is modeled by the standard k–ε model.

The rate of preflame oxidation at elevated initial pressures and temperatures is taken according to the simple relationship:

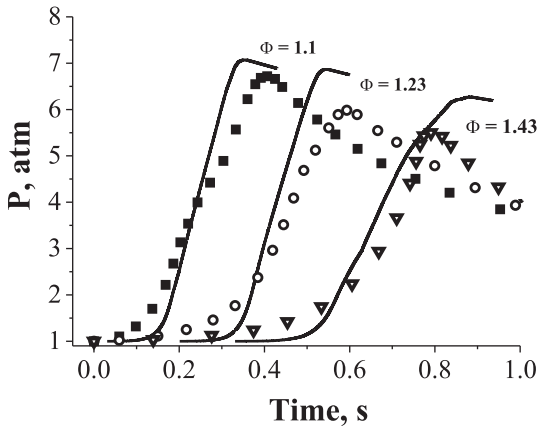

Fig. 7. Comparison between predicted (curves) and measured (symbols, Jarosinski et al., 2002) pressure histories.

$$w = -2.25 \cdot 10^{15} p^{-1.15} [H_2]^2 [O_2] e^{-\frac{24.000}{T}} \quad \text{(atm, mol, l, s)}$$

This relationship is obtained by fitting the ignition delays predicted by the validated detailed reaction mechanism of Basevich and Frolov (2007) with that provided by the single-stage mechanism:

$$H_2 + H_2 + O_2 \rightarrow H_2O + H_2O \tag{8}$$

Fig. 2a and b shows the performance of the single-stage mechanism of Eq. (8) in terms of the comparison with the ignition delay time predicted by the reaction mechanism of Basevich and Frolov (2007) at $p_0 = 1$ and 4 MPa, respectively.

Note that the single-stage mechanism of Eq. (8) is used solely for reducing the CPU time. As a matter of fact, for adequate simulation of preflame autoignition, a more sophisticated mechanism of hydrogen oxidation including chain-branching reactions should be applied.

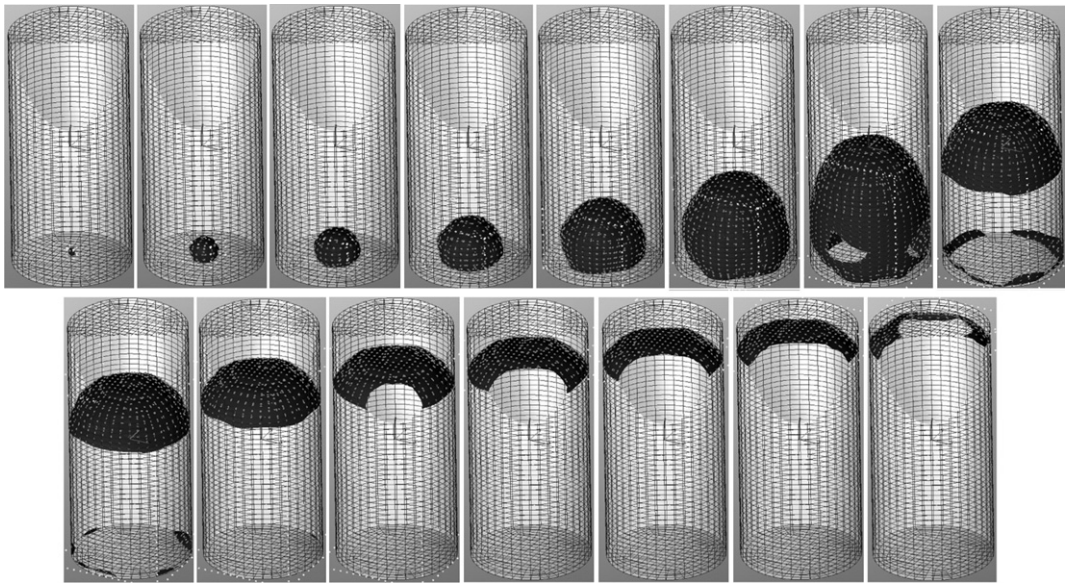

Fig. 6. Snapshots of predicted flame-front shape and position at different time instants after ignition (from left to right: $t = 5$, 15, 25, 35, 45, 55, 65, and 75 ms): cylinder height and diameter: 360 and 172 mm.

Table 4
Predicted (unstretched) laminar burning velocities (in cm/s) for stoichiometric n-heptane–air mixture at different initial pressures and temperatures.

T_0, K	p, atm				
	1	3	10	40	100
293	39	25	16	8.8	6
450	72	54	34	23	13
600	141	99	63	38	24
750	250	173	109	61	41
900	438	298	186	103	69

Two-dimensional calculations show that internal elements like corners and "doors" strongly affect the flow field in the enclosure producing turbulence and affecting flame propagation. Preflame autoignition occurs nearly simultaneously in the corners at both sides of the internal "room" wall (in the vicinity to monitoring locations #2 and #4 in Fig. 1) and is caused by the cumulative effects of the corners.

Fig. 3 shows the snapshots of the propagating flame. During first 3 ms the flame shape and position is insensitive to the existence of the "room". However, when the flame reaches the external corner of the "room," it starts to deform progressively: a flame tong forms at the "room door" and penetrates into the "room." The last snapshot in Fig. 3 corresponds to the time instant (4.5 ms) slightly preceding to preflame autoignition.

Let us consider in more detail the dynamics of autoignition in the vicinity to monitoring location #2 (see Fig. 1). Autoignition of precompressed and preheated hydrogen–air mixture ahead of the flame starts in several locations inside the "room" and spreads at the apparent velocity of ~50 km/s in the unburned region between flame and wall (Fig. 4). Obviously, this mode of flame propagation should be attributed to the induction or spontaneous flame (Zel'dovich, 1980). It is interesting that autoignition occurs closer to the "room" corner and walls rather than to the flame surface. This is caused by multiple reflections of pressure waves from the walls at the earlier stages of flame evolution in the enclosure and therefore more preferable conditions for mixture autoignition in the vicinity to the walls rather than to the flame. In 1 μs after the first autoignition events, nearly all mixture in the "room" is burned except for a thin near-wall layer where the temperature is somewhat lower. The border of the white "bulb" evident in Fig. 4 at time 1 μs and later corresponds to the flame-surface enveloping combustion products formed prior to preflame autoignition.

As could be expected, the autoignition pattern depends on the number of notional particles. However when the mean number of particles per computational cell is sufficiently large (on the level of 10–15 and more) this dependence becomes weak. The effect of computational grid on the autoignition pattern was also studied. The results for the grid with the mean cell size smaller by a factor of 2 were very close to those discussed herein.

The curve in Fig. 5a shows the predicted pressure history in the internal "room" corner (monitoring location #2). The predicted amplitude of the first pressure peak is about 10.4 MPa. Pressure histories in different monitoring locations are shown in Fig. 5b. The pressure-wave arising due to preflame autoignition traverses the enclosure and reflects from the walls giving rise to secondary pressure peaks with the intensity considerably exceeding the maximum static pressure at normal combustion.

4.2. Combustion of propane in cylindrical enclosure

Jarosinski, Podfilipski, Gorczakowski, and Veyssiere (2002) reported the results of combustion experiments with propane–air mixtures of different composition in a vertical vessel. The vessel was a cylinder 172 mm in inner diameter and 360 mm high made of Plexiglas. The vessel was fitted with an igniter at its bottom cover or in the center. The experiments were carried out with propane–air mixtures at the temperature of 293 ± 1 K. Both normal-gravity and microgravity tests were performed.

In the 3D computational example, all calculation settings are the same as in the example with hydrogen (see Section 4.1). Normal-gravity conditions are considered. Ignition is triggered at the bottom of the vessel.

For calculating the local instantaneous laminar flame velocities in propane–air mixtures, the look-up tables of Belyaev et al. (2010) are also used. As an example, Table 3 shows a fragment of such a look-up table for the stoichiometric propane–air mixture at different initial pressures and temperatures. The table has been also constructed based on the numerical solution of the problem of one-dimensional planar (unstretched) laminar flame structure with the validated overall reaction mechanism of propane oxidation of Basevich and Frolov (2006).

The preflame autoignition in propane–air mixtures is modeled using the same mechanism of Basevich and Frolov (2006) but with properly changed preexponential factor of a rate-limiting reaction. This mechanism is capable of predicting low-temperature multi-stage autoignition with cool flame and hot explosion.

Fig. 6 shows the snapshots of calculated flame-front shape and position at combustion of fuel-rich propane–air mixture with equivalence ratio $\Phi = 1.1$. Within the FT method, the flame is an infinitely thin surface separating fresh mixture from combustion products and is traced explicitly at the subgrid level. Therefore the flame front is not smeared and there is no numerical diffusion of flow parameters through it. The latter is very important for adequate modeling of preflame autoignition. The flame front is seen to initially elongate in vertical direction, however in the course of upward propagation it gradually flattens and becomes nearly plane at the end of the process. This behavior correlates well with experimental observations. In this example, no preflame autoignition was detected both in the experiments and in the calculations.

Fig. 8. Predicted snapshots of preflame autoignition at ~93 ms. Cylinder diameter is 172 mm.

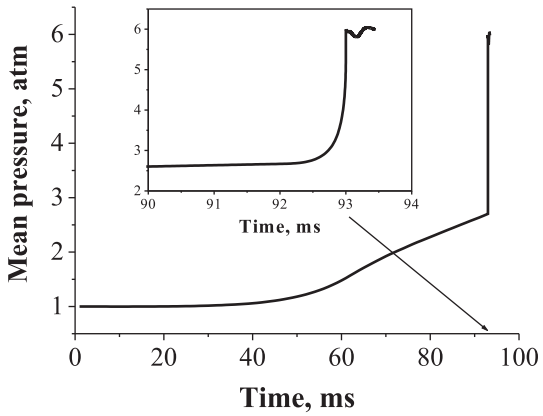

Fig. 9. Predicted time history of pressure in the cylindrical enclosure.

Fig. 7 compares predicted and measured pressure histories in the combustion vessel for three fuel-rich propane–air mixtures. The agreement between predicted and measured results can be treated as satisfactory despite combustion in experiments is seen to be less intense than in the calculations. Most probably, this effect can be attributed to poor modeling of heat loss to the bottom and lateral walls of the vessel (no grid refinement at the walls) and to the oversimplified model of the ignition stage (no ignition induced expansion of the combustion products, etc.). Note that in the present calculations we paid more attention to the modeling of combustion processes rather than to the adequate representation of heat loss and ignition. The agreement between predicted and measured pressure histories in Fig. 7 can be improved by the proper refinement of the computational grid in the vicinity to the walls and by better modeling of the ignition stage.

4.3. Combustion of n-heptane in cylindrical enclosure

To show the capability of the 3D FTP method of simulating both flame propagation and preflame autoignition, we have considered the same vertical cylindrical vessel as in Section 4.2 but initially filled with the homogeneous stoichiometric n-heptane–air mixture at initial pressure 1 atm and elevated initial temperature 500 K. All other settings were the same as in the examples with hydrogen (Section 4.1) and propane (Section 4.2). To avoid consideration of n-heptane condensation at cold walls, the wall temperature was taken equal to 400 K.

Similar to the example of Section 4.2, for calculating the local instantaneous laminar flame velocities in n-heptane–air mixtures, the look-up tables of Belyaev et al. (2010) were also used. Table 4 shows a fragment of the look-up table for the stoichiometric n-heptane–air mixture at different initial pressures and temperatures. The table has been also constructed based on the unstretched laminar flame data obtained with the validated overall reaction mechanism of n-heptane oxidation of Basevich and Frolov (2006).

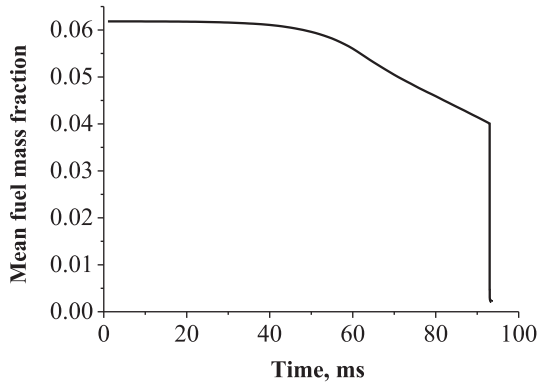

Fig. 10. Predicted time history of fuel mass fraction in the cylindrical enclosure.

The preflame autoignition in n-heptane–air mixtures was modeled using the validated overall reaction mechanism of Basevich and Frolov (2006) capable of predicting low-temperature multistage autoignition with cool flame and hot explosion.

The mixture was ignited at the symmetry axis near the bottom wall. After ignition, the flame propagated upward and the pressure in the cylinder increased. At the end of flame propagation (at time about 93 ms), preflame autoignition occurred in the upper part of the cylinder.

Fig. 8 shows the results of calculations in terms of the temperature iso-surface ($T = 735$ K). One can clearly see hot spots ahead of the propagating flame. Snapshots a, b, and c correspond to the same instant of time but to different directions of view. Note that the temperature in the hot spots at this instant of time exceeds the mean preflame temperature by only about 10 K. This temperature difference arises in the course of flow evolution in the enclosure under the effect of pressure waves generated by the propagating flame and multiple pressure-wave reflections from cylinder walls.

Preflame autoignition in the hot spots results in the abrupt pressure rise in the preflame zone and the formation of a blast wave propagating downwards. Fig. 9 shows the predicted pressure history in the vessel. Clearly, at ~93 ms there is a sharp pressure rise, followed by pressure waves in the vessel (see insert in Fig. 9). Complimentary Fig. 10 indicates that fuel in the preflame zone is depleted very quickly.

5. Concluding remarks

A novel computational approach based on the coupled 3D FTP method has been developed and used for numerical simulation of confined explosions with/without preflame autoignition. The method allows continuous monitoring of both flame front and preflame reactions with generation of high-intensity secondary pressure peaks and is applicable to simulations of accidental explosions in various industrial reactors with complex geometry.

Acknowledgments

This work was partly supported by the Russian Foundation for Basic Research (grant 11-08-01297) and AVL LIST GmbH.

References

Basevich, V. Y., & Frolov, S. M. (2006). Overall kinetic mechanisms for modeling multistage autoignition of hydrocarbons in reacting flows. *Russian Journal of Chemical Physics, 25*(6), 54–62.

Basevich, V. Y., & Frolov, S. M. (2007). Kinetics of `blue' flames in the gas-phase oxidation and combustion of hydrocarbons and their derivatives. *Russian Chemical Reviews, 76*(9), 867–884.

Belyaev, A. A., Basevich, V. Y., Frolov, F. S., Frolov, S. M., Basara, B., & Suffa, M. (2010). Data base for characteristics of n-heptane laminar combustion. In S. M. Frolov (Ed.), *Combustion and explosion* (pp. 30–37). Moscow: Torus Press, 3.

Bradley, D. (1992). How fast can we burn? *Proceedings of the Combustion Institute, 24*, 247–253.

Damkoehler, G. (1940). Der einfuss der turbulenz auf die flammengeschwindigkeit in gasgemischen. *Zs Electrochemie, 6*, 601–652.

Driscoll, J. F. (2008). Turbulent premixed combustion: flamelet structure and its effect on turbulent burning velocities. *Progress in Energy and Combustion Science, 34*, 91–134.

Frolov, S. M., & Ivanov, V. S. (2010). Combined flame tracking–particle method for numerical simulation of deflagration-to-detonation transition. In G. D. Roy, & S. M. Frolov (Eds.), *Deflagrative and detonative combustion* (pp. 133–156). Moscow: Torus Press.

Gülder, Ö. L. (1990). Turbulent premixed flame propagation models for different combustion engines. *Proceedings of the Combustion Institute, 23*, 743–750.

Ivanov, V. S., & Frolov, S. M. (2010). Mathematical modeling of flame propagation in smooth tubes and in tubes with regular obstacles. *Journal of Fire and Explosion Safety, 19*(1), 14–19.

Jarosinski, J., Podfilipski, J., Gorczakowski, A., & Veyssiere, B. (2002). Experimental study of flame propagation in propane–air mixture near rich flammability limits in microgravity. *Combustion Science and Technology, 174*, 21–48.

Liu, Y., Ziegler, M., & Lenze, B. (1993). *Proceedings of a joint meeting of the British – German Sections of the Combustion Institute* (pp. 64–67). Cambridge (UK).

Peters, N. (1986). Laminar flamelet concepts in turbulent combustion. *Proceedings of the Combustion Institute, 21*, 1231–1250.

Peters, N. (1999). The turbulent burning velocity for large scale and small scale turbulence. *Journal of Fluid Mechanics, 384*, 107–132.

Pope, S. B. (1985). PDF methods for turbulent reactive flows. *Progress in Energy and Combustion Science, 11*, 119–151.

Pope, S. B. (1990). Computation of turbulent combustion: progress and challenges. *Proceedings of the Combustion Institute, 23*, 591–612.

Shchelkin, K. I. (1949). *Fast combustion and spin detonation of gases*. Moscow: Voenizd.

Spalding, D. B. (1976). Mathematical models of turbulent flames, a review. *Combustion Science and Technology, 13*, 3–25.

Zel'dovich, Y. B. (1980). Regime classification of an exothermic reaction with nonuniform initial conditions. *Combustion and Flame, 39*(2), 211–215.

Zimont, V. L. (1979). Theory of turbulent combustion of a homogeneous fuel mixture at high Reynolds numbers. *Combustion, Explosion, and Shock Waves, 15*(3), 305–311.